

# Near Infra-Red Light Responsive Carbon Nanotubes@Mesoporous Silica for Photothermia and Drug Delivery to Cancer Cells

Bing Li<sup>1,2</sup>, Sébastien Harlepp<sup>3-5</sup>, Valentin Gensbittel<sup>3-5</sup>, Connor J. R. Wells<sup>1</sup>, Ophélie Bringel<sup>2</sup>, Jacky G. Goetz<sup>3-5</sup>, Sylvie Begin-Colin<sup>1</sup>, Mariana Tasso<sup>6</sup>, Dominique Begin<sup>2</sup>, Damien Mertz<sup>1,\*</sup>

<sup>1</sup>Institut de Physique et Chimie des Matériaux de Strasbourg (IPCMS), UMR-7504 CNRS-Université de Strasbourg, 23 rue du Lœss, BP 34 67034, Strasbourg Cedex 2, France, §

<sup>2</sup>Institut de Chimie et Procédés pour l'Energie, l'Environnement et la Santé (ICPEES), UMR-7515 CNRS-Université de Strasbourg, 25 rue Becquerel, 67087 Strasbourg, Cedex 2, France

<sup>3</sup>Tumor Biomechanics, INSERM UMR\_S1109, Strasbourg, France,

<sup>4</sup>Université de Strasbourg, Strasbourg, France.

<sup>5</sup>Fédération de Médecine Translationnelle de Strasbourg (FMTS), Strasbourg, France.

<sup>6</sup>Instituto de Investigaciones Fisicoquímicas Teóricas y Aplicadas (INIFTA), Departamento de Química, Facultad de Ciencias Exactas, Universidad Nacional de La Plata - CONICET, Diagonal 113 y 64, 1900 La Plata, Argentina.

E-mail : [damien.mertz@ipcms.unistra.fr](mailto:damien.mertz@ipcms.unistra.fr)

**Keywords :** Phototherapy ; NIR-Light Induced Drug Delivery; Carbon Nanotubes; Mesoporous Silica Coatings , Nanocomposite Hydrogels, Cancer Cells.

**ABSTRACT.** Among smart activable nanomaterials used for nanomedicine applications, carbon-based nanocomposites are well known to ensure phototherapy while their use for controlled drug delivery is still rarely investigated. In this work, original hybrid mesoporous silica (MS)-coated carbon nanotubes (CNTs) nanoplatforms have been designed to provide phototherapy combined with drug release mediated by NIR laser excitation. The responsive CNT@MS are chemically modified with original isobutyramide (IBAM) grafts acting as non-covalent binders, which ensure a very high drug loading capacity ( $\geq$ to 80 wt%) of the antitumor drug doxorubicin (DOX) as well as the final adsorption of a human serum albumin (HSA) shell as biocompatible interface and drug gate-keeping. The drug is demonstrated to unbind from the nanocomposite only upon photothermal excitation and to release in the solution. Such smart platforms are further shown to deliver drug upon several pulsatile NIR excitations with controlled temperature profiles. Regarding antitumor action, we demonstrate here that the NIR light induced photothermic effect from the nanocomposites is the main effect accounting for cancer cell toxicity and that DOX delivery mediated by the NIR light brings an additional toxicity allowing a synergistic effect to efficiently kill tumor cells. Finally, when our nanocomposites are embedded within a hydrogel mimicking extracellular matrix, the resulting smart responsive scaffolds efficiently release DOX upon NIR light to the cells localized above the composite hydrogel. These results demonstrate that such nanocomposites are highly promising as new

components of implantable antitumor scaffolds that are able to respond to external stimuli in time and location for a better disease management.

## INTRODUCTION

The development of smart multi-functional nanocomposites capable of releasing therapeutic molecules under various external stimuli has become a major challenge in recent years in the biomedical field. These nanocomposites are designed to be either injected as circulating objects [1–6] or implanted *in situ* in a polymer support matrix [7–12] for the treatment of different types of tumors. Another challenge now is the design of multifunctional nanoplateforms (NPFs) able to combine, in one formulation, two or more functionalities, e.g. simultaneous therapy and diagnostic (theranostic) for real-time therapy monitoring, and synergic action of two or more therapeutic approaches.

In the field of tissue engineering, the incorporation of activable inorganic materials (e.g. iron oxide, gold or carbon materials) into polymer scaffolds (e.g. hydrogels or electrospun fibers) is a way to formulate new composite materials that would be used as smart implants or integrated devices in the body.[13–15] The advantages to add remote responsive NPs into such polymer matrix are: i) improved mechanical properties; ii) the response to external stimuli (near infrared light, mechanical force, electric or magnetic field, etc.); iii) the eventual clinical imaging property (MRI, X rays, etc), and iv) encapsulation of the activable material into a biocompatible scaffold, thus preventing material-related toxicity issues. In this work, we report on the design and use of drug-loaded carbon-based composites incorporated in a biocompatible hydrogel mimicking the extracellular matrix (ECM).

Among the different materials needed to produce such activable nanocomposites, carbon-based materials are promising materials.[16–18] Besides their exceptional mechanical and electrical conductive properties, they are able to release heat under near-infrared radiation by vibrational relaxation of graphite structures in the near infrared (NIR) range (750-1400 nm). Given the relative transparency of biological tissues in the NIR optical window, this property is of huge interest for combining both phototherapy and remotely activable drug delivery under such external stimuli.[19–23] Indeed, the use of infrared light to trigger the release of an active ingredient locally could be of great interest in the treatment of tumors because of its easier implementation than other sources of radiation (X-ray scanner, gamma radiation, magnetic waves, etc.). However, the design of carbon-based composites for biomedical applications endowed with phototherapy and remote drug delivery faces important challenges as follows. Main issues with CNTs are their asbestos form factor (very long length-to-diameter ratio) and the inherent hydrophobicity of carbon leading to self-aggregation in biological medium.[24–26] To solve these problems, newly processed CNTs with a better form factor were developed.

Several fractionation and split treatments decrease the form factor of these carbon nanotubes, such as mechanical grinding (length of about less than 500 nm), or CNT compression induced by ultrasonic effects [27] or by harsh acidic treatment of CNTs [28].

Besides, CNTs can be rendered hydrophilic by the cutting treatment which introduces hydroxyl groups or by a post-functionalization.[19,20,29] A capping layer playing the role of drug reservoirs may also be obtained by the surface modification with various polymers[30–33] or chemical groups[20] or by the deposition of a uniform layer of porous silica [34–36]. Among current coating layers for drug loading, mesoporous silica (MS) shells are particularly attractive materials as they are robust, biocompatible, hydrophilic, easily chemically modified and have a high drug delivery capability thanks to their important pore volume and after a suitable surface functionalization.[37]

Recently, we and coworkers developed various functionalized MS NPs having well-controlled pore sizes (from 2 to 15 nm) [38,39] and translated these approaches to coat CNTs but also iron oxide NPs with various MS shell nanostructures [40–43]. Especially small pore MS around CNTs allowed loading of such nanocomposites with doxorubicin, (DOX, an antitumor anthracycline molecule with antimitotic action by DNA intercalation) with increased rates (up to several times the mass of the carrier) when compared to past work [42]. However, different issues were raised in this previous work: i) the loading of DOX was initially performed at an aminosiloxane surface which is not optimal for biomedical applications given its high surface charge and marked fouling, ii) the drug release was activated with a quite high laser power (6 W/cm<sup>2</sup>) which may lead to overheating in a biological medium; iii) these nano-composites were also shown to release a moderate proportion of immobilized DOX under near IR radiation (1064 nm) and iv) no functional study on cells was done with these systems.

Herein, to address these issues, we designed a new class of functional CNT@MS nanocomposites (**Figure 1**). First, the CNTs are processed in acidic conditions to afford sliced CNTs with a more suitable size distribution adapted for medical applications. Their coating by a MS shell having small pore size (*ca.* 3 nm) is performed with a precise control over silica shell thickness. Then, we used here the grafting of IBAM groups to ensure high drug loading and a final protein capping. Indeed, IBAM groups grafted at silica surfaces were reported previously to be versatile non-covalent surface binders of a range of proteins through a single step adsorption. [44–46]. Here, IBAM grafts at silica surface are assessed for the first time to load DOX through non-covalent interactions followed by HSA coating to ensure a good integrity of the nanocomposites. We assumed here that IBAM grafts play the role of a thermoresponsive interface that unbind the loaded drugs from the surface upon the photo-induced local heating generated from the underneath CNTs. Hence, we address here the full characterization of CNTs@MS nanocomposites and of DOX loading and subsequent HSA wrapping on

CNTs@MS@IBAM and we investigated the efficiency of drug release upon NIR light application. Various drug profiles as a function of time, concentration, and laser power are provided demonstrating the possibility for NIR light remote release.

In the last step of this design, with the aim to create a drug releasing scaffold upon NIR light exposure, the drug loaded nanocomposites CNTs@MS@IBAM-DOX@HSA are formulated within a hydrogel made of various extracellular matrix biopolymers (Matrigel, ECM-like hydrogel) often used in biomaterials field.[47–49] The development of such hydrogel nanocomposites is very attractive for antitumor and tissue engineering applications. Indeed, the scaffold can display some advantages over circulating NPs, such as limiting macrophage uptake, or decreasing the drug loss (or the non-targeted drug delivery) by injecting the scaffold in the diseased site and thus avoiding sides effects.

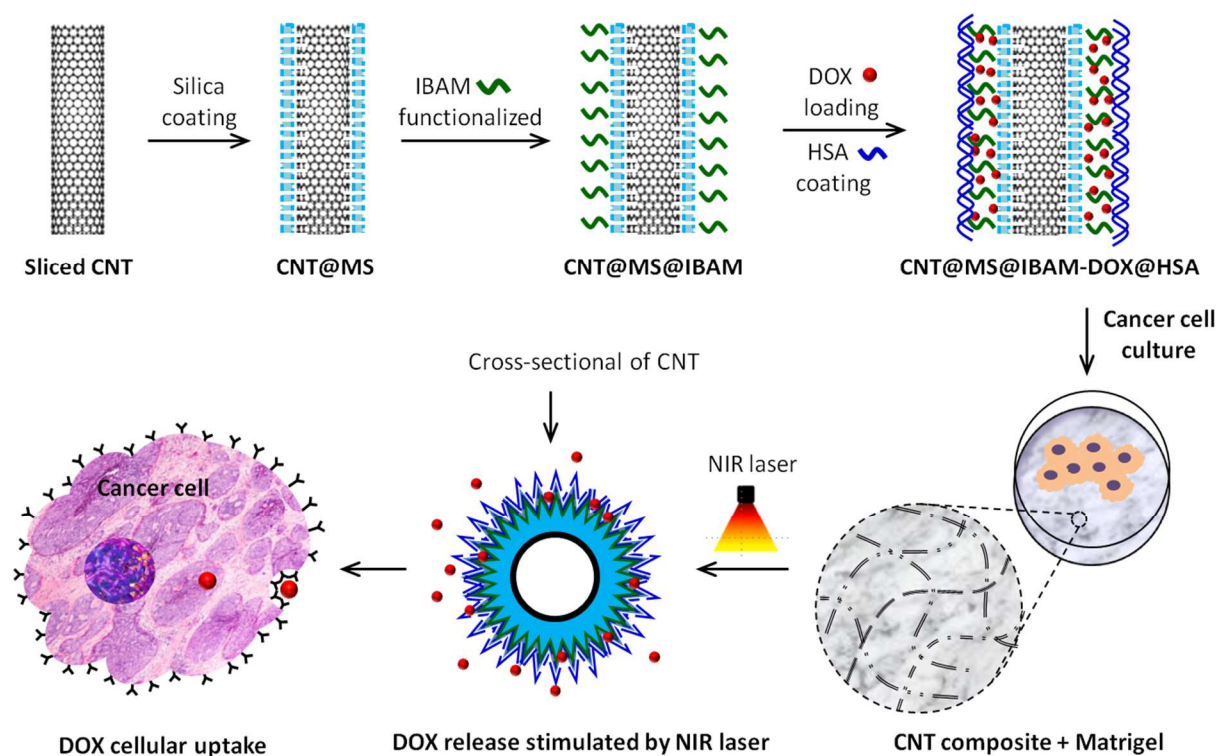


**Figure 1.** Scheme describing the formation of the CNT@MS@IBAM-DOX@HSA nanoconstructs and their formulation into a hydrogel assessed with breast cancer cells.

## Materials and Methods

### Chemicals.

Carbon nanotubes PR-24-XT-PS (CNTs) were supplied by Pyrograf-III. Cetyltrimethylammonium bromide (CTAB) was obtained from Roth (France). Nitric acid (HNO<sub>3</sub>), sulfuric acid (H<sub>2</sub>SO<sub>4</sub>), ethanol (EtOH), tetraethyl orthosilicate (TEOS), sodium hydroxide (NaOH), ammonium nitrate

( $\text{NH}_4\text{NO}_3$ , >99%), 3-aminopropyltriethoxysilane (APTS), isobutyryl chloride (IBC), triethylamine ( $\text{Et}_3\text{N}$ ), dimethylformamide (DMF), dimethylsulfoxide (DMSO), sodium bicarbonate ( $\text{NaHCO}_3$ ), human serum albumin (HSA, >97%) and fluorescein isothiocyanate (FITC) were obtained from Sigma-Aldrich (France). Doxorubicin hydrochloride (DOX, purity 99%) was purchased from OChem Incorporation (France). Ammonium hydroxide solution (25% in  $\text{H}_2\text{O}$ ) was obtained from Fluka. The MTS reagents CellTiter 96® AQueous were obtained from Promega. The D2A1 cells were seeded and grown up at 37°C at 5%  $\text{CO}_2$ , using DMEM high glucose medium supplemented with with 5% NBGS, 5% FBS, 1% NEAA-MEM, 1% Penstrep (Sigma Aldrich). For 2D or 3D growth the cells were seeded into either an opaque-walled 96 well plate (Fisher scientific) or a 15 well plate suited for 3D cell culture (Ibidi). The Membrane Matrix used to built the 3D scaffold was obtained from Thermo Fisher Scientific.

## Procedures.

**Synthesis of cleaved CNTs.** The acid treatment was performed by adding 0.75 g of CNTs into a mixture of  $\text{H}_2\text{SO}_4/\text{HNO}_3$  (3:1, 108 mL) and then bath sonicated (Bandelin SONOREX RK 255 S) for 24 h under at 0 °C. After this time, 100 mL of NaOH aqueous solution (10 M) was added dropwise into the acidic black suspension for neutralization, and finally the mixture was adjusted to neutral by the dropwise addition of NaOH (1 M). The CNTs were then centrifuged (13000 g, 13 min, Eppendorf Centrifuge 5804 R) and washed with distilled water (twice with 25 mL each). After washing, the CNTs were reduced at 900°C for 2 h with a heating ramp of 10 °C/min under argon. The resulting material was used as the initial material for the following functionalization procedures.

**Synthesis of mesoporous silica coated CNTs.** In a typical procedure, 372 mg of CTAB was added into a mixture of  $\text{H}_2\text{O}$  (90 mL) and EtOH (60 mL) with stirring at 60 °C for 2 h. 72 mg of CNTs were dispersed in the CTAB solution by ultrasonication (2 x 20 min, power = 750 W, amplitude = 40%, temperature = 30 °C, runs: 50" ON, 50" OFF, Vibracell 75043 from Bioblock Scientific), yielding a black suspension. The sol gel process was initiated after addition of TEOS (180  $\mu\text{L}$ ) and NaOH (180  $\mu\text{L}$ , 1M) into the above mixture. The mixture was stirred for 16 h at room temperature. Finally, the composite was centrifuged and washed with EtOH (2 x 25 mL, 12000 g, 12 min) and re-dispersed in EtOH. The process resulted in the formation of a uniform layer of silica on every individual CNT.

**CTAB extraction from CNT@MS composite.** The removal of mesostructural templating agent CTAB from the silica pores was done by mixing the CNT@MS composite with 25 mL  $\text{NH}_4\text{NO}_3$  (20 mg  $\text{mL}^{-1}$  in EtOH) under 60 °C with stirring for 1 h. The surface charge of CNT@MS was

measured by Zeta potential after each washing, in order to make sure that the majority of CTAB was removed. This process was repeated approximately 5 times.

**CNT@MS surface modification with aminopropyltriethoxysilane APTS.** 50 mg of CNT@MS were dispersed in 27 mL of EtOH. Then, 1.2 mL of NH<sub>4</sub>OH (25 % in water) and 5 mL of APTS were added respectively and the mixture was agitated on a mechanical wheel (40 rpm) at room temperature for 2 h. After that, the amino-modified composite was centrifuged and washed with EtOH (2 x 20 mL, 13000 g, 14 min). The composite after APTS modification was denoted as CNT@MS@APTS.

**CNT@MS surface functionalization with IBAM moieties.** In a typical procedure, the resulting CNT@MS@APTS composite was washed and centrifuged with 20 mL DMF (13000 g, 13 min). Once the supernatant had been removed, a mixture of 1.2 mL Et<sub>3</sub>N and 1.5 mL DMF was added. The mixture was vortexed for 10 s before the addition of 1.65 mL of IBC pre-mixed with 1.5 mL of DMF. The reaction was left on the mechanical wheel for 1 h 30 min. After this time, a small volume of water (*ca.* 1-2 mL) was added to dissolve the precipitate formed by the reaction. This was followed with centrifugation and washing at 13000 g for 14 min (1 x 20 mL wash in DMF, 1 x 20 mL wash in H<sub>2</sub>O). The composite at this point was denoted as CNT@MS@IBAM.

**Impregnation of doxorubicin.** Typically, 2.5 mg of CNT@MS@IBAM after surface functionalization were dispersed in 1 mL of DOX aqueous solution at a given concentration and agitated on a mechanical wheel (40 rpm) for 16 h. After impregnation, the mixture was centrifuged (13000 g, 10 min) and 400 µL of the supernatant were mixed with 3.6 mL of H<sub>2</sub>O to obtain a solution diluted 10 times. The composite was denoted as CNT@MS@IBAM-DOX. The DOX loading capacities were calculated by measuring the UV/Vis spectra (Lambda 950 UV/VIS Spectrometer by Perkin Elmer) of the diluted supernatant. A series of additional washes with water (3 x 1 mL) were implemented to remove loosely-bound impregnated DOX prior HSA modification (as follows).

**FITC labeling of HSA.** 531 µL of fluorescein isothiocyanate (10 mg mL<sup>-1</sup> in DMSO) were mixed with 30 mL of HSA (10 mg mL<sup>-1</sup>) in sodium bicarbonate buffer (NaHCO<sub>3</sub> 0.1 M, pH 8.5). The mixture was stirred overnight and then dialyzed (membrane pore size: 10 kDa) in MilliQ water to remove free FITC. Finally, the concentration of HSA<sup>FITC</sup> was adjusted to 10 mg mL<sup>-1</sup> in water for further use.

**HSA coating.** 6.4 mg of CNT@MS@IBAM-DOX composite after surface functionalization and DOX impregnation were dispersed in 3 mL HSA at a concentration of 0.21 mg mL<sup>-1</sup>, then the mixture was stirred on a mechanical wheel for 1 h. Afterwards, the solution was centrifuged and washed with H<sub>2</sub>O (2 x 2 mL, 13000 g, 13 min). The composite was denoted as CNT@MS@IBAM-

DOX@HSA. The supernatant was measured with UV/vis spectroscopy to detect the mass loss of DOX during this step.

**DOX release stimulated by NIR laser.** To study the release of DOX under NIR irradiation, 1 mL of a given concentration of CNT@MS@IBAM-DOX@HSA solution (DLC ca 58%) was placed in a 1 mL plastic cuvette and then irradiated with the 1064 nm laser with power densities at either 1 or 2.5 W.cm<sup>-2</sup>. For every trial, the sample was exposed to NIR light for 15 min, followed by a break lasting 3 days at 4°C. The mixture was centrifuged after this period and the released DOX in the supernatant was removed and measured by UV/vis spectrometry to determine the amount of DOX released. Then 1 mL of fresh water was added and the composite was dispersed by 10 s of sonication and stored in a 4 °C refrigerator. Regarding pulsatile assay, the same procedure was applied: the samples were passed for the next NIR exposure and rest period and so on for four times. The cumulative DOX release is the sum of each trial of DOX release.

#### **Cell culture and NIR exposure setup for in vitro experiments.**

**D2A1 cells (CVCL\_0190).** Mouse mammary carcinoma (BALB/c female). Major information on the D2A1 cell line can be found following this link: [https://web.expasy.org/cellosaurus/CVCL\\_0190](https://web.expasy.org/cellosaurus/CVCL_0190). Culture conditions: 37°C/5% CO<sub>2</sub>. DMEM HG with 5% NBCS, 5% FBS, 1% NEAA-MEM, 1% Penstrep.

**Bidimensional cell proliferation and viability assays.** D2A1 cells were seeded (8000 cells per well in 50µl of DMEM) in each of the wells of the opaque 96 well plate and incubated at 37 °C in 5% CO<sub>2</sub> for 45minutes to an hour to allow the cells to adhere [50,51]. Then, DMEM medium (150 uL) supplemented with the final concentration of CNT@MS@IBAM@HSA or CNT@MS@IBAM-DOX@HSA suspensions were introduced and incubated at 37°C, 5% of CO<sub>2</sub> for 24h. NIR irradiation (at 1W.cm<sup>-2</sup> for 15 minutes) was applied and the cells were further incubated at 37 °C in 5% CO<sub>2</sub> for 24 h. NIR irradiation was performed with a homemade setup. The illumination was performed from the top cover towards the well. Cell Titer Glo (Promega) reagent was then added to each well (20 uL) followed by one-hour incubation at room temperature, allowing cell lysis to be completed and luciferin to be oxidized by the cellular ATP. The 96 well plate was introduced into a plate cell reader (SpectraMaxID5 from MolecularDevices) and luminescence was collected. The intensity of control wells (cells without CNTs called Luminescence Control) were used to normalize the luminescence values (all values are between 0 and 1, value of the control wells). We checked the luminescence values from wells filled with medium and the values were at the noise level, therefore we decided to not correct with these values. Nevertheless, CNTs have a black aspect and therefore have the ability to absorb part of the emitted light from the viability experiments such as for Optical density

filters. We, thus, characterized the part of absorbed light. We cultured different wells with 8000 cells per well for 48h in normal cell growth conditions. Before running the Cell Titer Glo experiment, we first added the 4 studied concentrations of CNT@MS@IBAM@HSA in different wells. This short time where the CNTs were in contact with the cells is assumed to only affect the emitted light. As shown on figure S6B. we observe that only  $\approx 23\%$  of the luminescence is collected. Therefore, we used the average values of what we introduce as Absorption for the different concentrations of CNTs to correct all the signals measured in presence of CNTs. Using the mathematical formulation we can write:

$$Relative\ Viability = \frac{Measured\ luminescence}{Luminescence\ Control} \times \frac{1}{Absorption}$$

**Short time 3D cell culture and DOX cellular uptake after NIR irradiation.** To study the cellular uptake of DOX upon NIR irradiation, a 50  $\mu\text{l}$  total volume of Matrigel with a given concentration of CNT@MS@IBAM-DOX@HSA or CNT@MS@IBAM@HSA composite were mixed and coated before subsequent cell seeding. D2A1 cells were incubated for 24 h and subjected to laser irradiation of  $1\text{W}\cdot\text{cm}^{-2}$  for 15 minutes. NIR-illuminated cells were cultivated for an additional 24 h before assessing DOX release. NIR irradiation was performed for 15 minutes at power density of  $1\text{W}\cdot\text{cm}^{-2}$ . DOX release/delivery was characterized using a Leica SP5 confocal microscopy. To follow intracellular DOX fluorescence, we excited the sample at 488 nm (argon laser) and collected the fluorescence on a broad range in emission from 520 to 650 nm on stacks of images with steps in z of about 400nm. Each image from the stack was then analyzed with Image J and the average intensity from the cell with respect to its area in each plane was computed. Thus we could address the intensity distribution or the average signal from a single cell or cluster of cells.

**Longer time 3D cell culture in presence of CNT@MS.** To study the toxicity linked to the presence of CNTs embedded in a 3D scaffold close to the tumor cells, a 50  $\mu\text{l}$  total volume of Matrigel with a given concentration of CNT@MS@IBAM-DOX@HSA or CNT@MS@IBAM@HSA composite were mixed and coated before subsequent cell seeding. murine breast carcinoma cells labelled with Nuclear Localization Signal fused with Green Fluorescent Protein (D2A1, n=8000) were added on top of the gel and again incubated for 5 days allowing the growth of tumor spheroids[52]. The cells were grown in 3 different conditions. In the first condition, cells were seeded on just Matrigel without any CNT@MS. In the second condition  $2.5\text{ mg mL}^{-1}$  CNT@MS@IBAM@HSA-Fitc complemented the Matrigel composition, whereas in the last condition  $2.5\text{ mg mL}^{-1}$  CNT@MS@IBAM-DOX@HSA was added. Upon 5 days of culture, tumor spheroids were imaged under the confocal microscope.



**Statistical analysis.** Statistical analysis of the results obtained were performed using the GraphPad Prism program version 5.04. The Shapiro-Wilk normality test was used to confirm the normality of the data. For data not following a Gaussian distribution, the Mann-Whitney test was used.

### **Characterization Methods**

**TEM microscopy.** Morphologies of the different nanocomposites were characterized by transmission electron microscopy (TEM) with a JEOL 2100 ultra-high-resolution microscope operating at 200 kV. The sample was first dispersed in EtOH and then we deposited 2 drops of the nanocomposite solution on a carbon-coated copper grid. The thickness of the silica shell was determined using Image J software on the TEM pictures. Results are indicated as mean layer thickness (nm)  $\pm$  standard deviation (nm).

**Zeta potential.** Zeta potential measurements at different synthesis stages were measured by using a Zetasizer nano ZS by Malvern Instruments. The measurements were performed by diluting 10  $\mu$ L of a nanoparticles' suspension in 1 mL water using a DTS1070 folded capillary cell. The pH of the measured solution was adjusted with HCl (100mM) and NaOH (100mM) aqueous solution.

**Nitrogen adsorption / desorption analysis.** Specific surface area of the silica coated CNTs was characterized by N<sub>2</sub> adsorption/desorption analysis and was calculated by the Brunauer-Emmett-Teller (BET) method. The pore size and pore volume were calculated by the Barrett-Joyner-Halenda (BJH) method. All the measurements were done on a Tristar 3000 Gas Adsorption Analyzer by Micromeritics Instruments. Before the tests, the samples were outgassed under vacuum at 150°C for about 4h.

**Thermal gravimetric analysis (TGA).** TGA was performed with a Q5000 Automatic Sample Processor by TA Instruments. The sample was dried in an oven at 150 °C for 24 h to remove the solvent and water before the TGA analysis. The runs were started from room temperature to 800 °C at a heating rate of 10 °C/min under air with a flow rate of 25 mL/min.

**UV/Vis spectroscopy.** UV-vis spectroscopy was used to determine the amount of drug loaded and released. The UV-vis spectra were recorded with a Lambda 950 UV/vis Spectrometer by Perkin Elmer. The solutions and the quartz cell were always protected from light using aluminum foil until the measurements were done.

**Confocal microscopy.** Microscopy of tumor cells was performed on a Leica SP5 confocal microscope. Samples were imaged with a 40X oil immersion objective. DOX was excited with a single 488 nm wavelength, and the emission was collected between 520 and 650nm. All the

image intensities were further analyzed and processed with the Image J software. For instance, the procedure to obtain figure 9B and C is described in figure S8.

## Results and Discussion

### 1. Synthesis of mesoporous silica coated carbon nanotubes

In a first step, the commercial CNTs were sliced from the microscale to the nanoscale using a solution of sulphuric and nitric acids. This acidic treatment increased the number of oxidative functional groups on the surface of the CNTs, resulting in break points which led to mechanical cleavage. NaOH was then used to neutralize the CNTs, followed by washings to subtract the salts produced. Then the CNTs oxygenated groups on the outer surface were reduced under a flow of argon in an oven at 900°C for 2 hours. The average length of the nanotubes was found in a range of 100 – 1000 nm, using transmission electron microscopy (TEM) whereas the initial CNTs had lengths of several tens of microns (in the range of 50-200 microns) (**Figure 2.A and B** before and after reduction).

Then a MS shell was coated around the CNTs using a modified procedure from Bian et al.[36]. A solution of cetyltrimethylammonium bromide (CTAB), water and ethanol was heated to 60 °C for 2 h. CTAB is a well-known surfactant that forms positively charged micelles in solution. When CNTs are dispersed in this mixture and given the hydrophobicity of heat-treated CNTs, the micelles arrange around the carbon nanotubes. The sol gel process begins upon addition of tetraethyl orthosilicate (TEOS) and NaOH. NaOH catalyzes the hydrolysis of TEOS, which condenses into silicate polyanions, leading to further condensation reactions, forming a network of Si-O-Si bonds. Once this MS structure is obtained, surfactant extractions are necessary to remove the CTAB from the pores of the silica. This was achieved with  $\text{NH}_4\text{NO}_3$ ; Zeta potential (ZP) measurements allowed to monitor the surface charge change from positive to negative. Five extractions were required to reach a stable negative zeta potential value indicating the completion of the process. The composites from this point onwards will be referred to as CNT@MS. TEM images showed homogenous coverage of the CNT@MS (**Figure 2.C**) on almost all the CNTs and a zoomed image (**Figure 2.D**) indicated the well-organized mesoporous structure of the MS shell around the CNTs. TEM images were used to establish the thickness of the MS shell, which was of  $30 \pm 4$  nm.

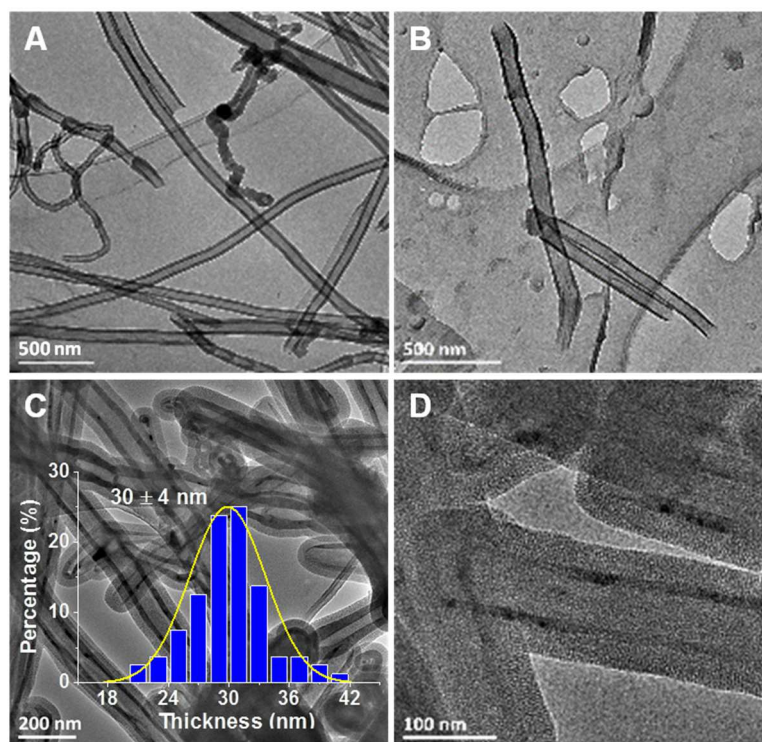


**Figure 2.** Representative TEM images of A) uncleaved CNTs. B) Acid-treated sliced CNTs. C) CNT@MS in a large area associated with the silica layer thickness distribution and D) CNT@MS in a zoomed image showing the mesoporous structures.

The porosity was investigated by nitrogen adsorption-desorption isotherms. **Figure S1** shows the nitrogen adsorption-desorption isotherm curves which exhibit a type IV isotherm, characteristic of mesoporous materials and which was used to calculate the surface area, pore size and pore volume. The Brunauer-Emmett-Teller (BET) surface area was thus calculated as  $594 \pm 14 \text{ m}^2 \text{ g}^{-1}$  and the pore size was found to be of *ca.* 3.4 nm with a pore volume of  $0.53 \text{ cm}^3 \text{ g}^{-1}$ . These data are consistent with the results obtained by Bian *et al.*[36], and in our previous studies [41,42]. Thermogravimetric analysis (TGA) was used to determine the C/SiO<sub>2</sub> composition of CNT@MS (**Figure 3. A**). The analysis of the curve indicated that CNTs started to decompose into CO<sub>2</sub> from 400 to 600 °C. This allowed us estimating a C/SiO<sub>2</sub> mass ratio of 63/37 for the CNT@MS composite system.

## 2. Surface functionalization with APTS and IBAM moieties

Next, after CTAB extraction from the pores, the surface of the MS was modified with APTS according to a standard process of multilayered siloxane condensation adapted from Wang *et al.* [53] and thereafter reacted with isobutyrylchloride (IBC) molecules to form grafted isobutyramide (IBAM) moieties[54] (**Figure 3.A**). For that, the CNT@MS were first dispersed in ethanol, and then a catalytic amount of NH<sub>4</sub>OH was added followed by 3-

aminopropyltriethoxysilane (APTS). The presence of  $\text{NH}_4\text{OH}$  allowed the APTS to condense on the silica surface over a 2 h period. The amine-functionalized silica surface was then further modified with isobutyrylchloride (IBC) resulting in IBAM functional groups on the outer surface of the silica shell. In previous works, IBAM moieties were, in particular, proved to non-covalently bind human serum albumin (HSA) and other proteins at the surface of MS carriers, leading to a tight biomacromolecular shell [41,43–45]. The APTS and IBAM grafting steps were characterized by TGA (**Figure 3.B**). TGA on the bare CNT@MS was used as a baseline and the TGA of CNT@MS@APTS and CNT@MS@IBAM allowed estimating by subtraction the amount of grafted aminosilane and then of the IBAM moieties. As can be seen, decomposition of APTS is achieved in the T range 300-450 °C and the weight loss was estimated at 10.4% of CNT@MS. Similarly, the IBAM grafts decomposition was overlapped with the APTS one and, by subtraction, the mass of IBAM decomposition was estimated at 7.0% of CNT@MS. TGA results of these hybrids enabled us to evaluate the grafting density: the number of APTS and IBAM molecules grafted on the silica surface was calculated to be of ca. 3.0 and 2.0 molecules per  $\text{nm}^2$ , respectively.

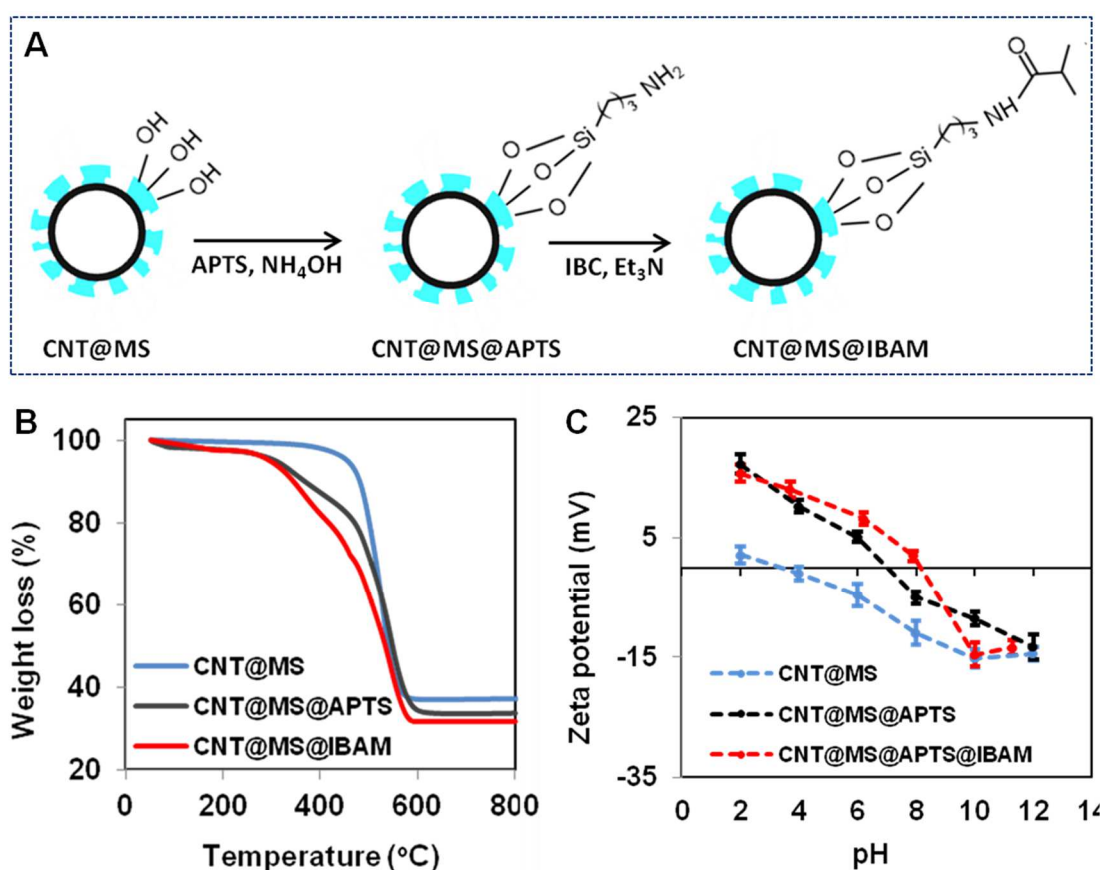


**Figure 3.** A) The process of reactions for CNT@MS@APTS and CNT@MS@IBAM composite. B) TGA curves of CNT@MS, CNT@MS@APTS and CNT@MS@IBAM. C) Zeta potential measurements of CNT@MS, CNT@MS@APTS and CNT@MS@IBAM as a function of pH value.

The surface functionalization steps of the MS layer were also investigated by zeta potential (ZP) measurements in water (**Figure 3.C**). The ZP curves as a function of pH value for bare CNT@MS and CNT@MS modified with APTS and IBAM moieties were thus traced. The ZP being the electrical potential at the slipping plane of the double ionic layer of the coated surface, gives in a first approximation indication of the surface charge changes. An iso-electric point (IEP) of ca. 2-3 was found on bare CNT@MS, consistent with the IEP value of bare silica surface chemistry as reported in the literature. After APTS modification, the ZP curve shifted towards higher pHs inducing a shift of the IEPs from ca. 3 for bare CNT@MS to a ca. 7 for the APTS-modified CNT@MS. This is consistent with the APTS presence on the silica surface providing a positive ammonium charge. After IBAM modification, CNT@MS@IBAM, the ZP curve was again shifted to higher pH and displayed an IEP of around 8, which indicate that a fraction of APTS moieties still remain after the reaction. Hence, overall, the TGA and ZP results evidenced that the surface of CNT@MS was effectively chemically modified with APTS and IBAM.

### 3. Drug loading and HSA coating

As we aimed at loading the CNT@MS@IBAM with an antitumoral agent (DOX) and then wrapping them with a serum albumin capping to ensure a biocompatible surface, our strategy was to adsorb DOX directly onto IBAM followed by the HSA coating. Firstly, this required investigating the loading in water of the hydrophilic DOX within the porous structure modified with IBAM groups. DOX displays strong absorption characteristics at 480 nm that allows its suitable detection and to quantify its adsorption. A UV/vis calibration curve of DOX in water measuring the absorbance at 480 nm at different DOX concentrations was plotted (**Figure S2**). For different [DOX] concentrations in water, an impregnation (during 16 hours) of the drug within CNT@MS@IBAM was carried out to load the composite. The suspensions were then centrifuged, and the resulting supernatants were dosed by UV/Vis spectroscopy to determine the mass of DOX that stayed outside of the composite. From that, the mass of DOX that entered the composite could be calculated. The drug loading capacity (DLC) and the drug loading efficacy (DLE) were used as loading parameters to establish the amount of drug within the composites. Their expressions are given below.

$$\text{DLC}\% = \frac{\text{weight of DOX loaded}}{\text{weight of CNT@MS}} \times 100\%$$

$$\text{DLE}\% = \frac{\text{weight of DOX loaded}}{\text{weight of DOX initial}} \times 100\%$$

Evolutions of these both parameters were plotted along with [DOX] (see DLC and DLE curves respectively in **Figure 4.A** and **4.B**). As can be seen in **Figure 4.A**, the DOX DLC increased

with the increasing concentration of DOX from 0.25 to 8 mg mL<sup>-1</sup>. At a concentration of 8 mg mL<sup>-1</sup> DOX<sub>(aq)</sub> solution, the DLC reached 68%, equivalent to 0.68 mg DOX per mg of CNT@MS. Interestingly, looking at the efficiency of the drug impregnation process, the DLE remained constant with the various concentrations, maintaining around DLE=23% regardless of the DOX concentration (**Figure 4. B**). This composite seems to behave as a loading matrix which ensures a concentration independent partition between DOX molecules in and outside of the composites. For the subsequent adsorption of a human serum albumin (HSA) shell, three times washes and centrifugation was required to completely remove the free DOX from the supernatant, which also resulted in the spontaneous leaking of the loosely-bound loaded DOX decreasing the DLC from 68% (impregnation by UV vis) to 58% (after washing steps by UV vis).

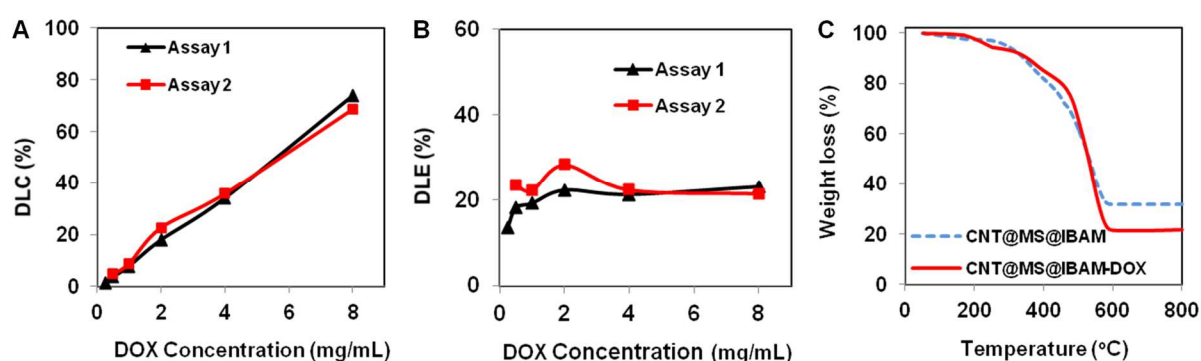


**Figure 4.** A) DLC and B) DLE curves as a function of DOX concentration in water. C) TGA curves of CNT@MS@IBAM and CNT@MS@IBAM-DOX (DLC= 56% after washing steps)

The DOX loading amount was also evaluated by TGA analysis performed directly on the nanocomposite after the three washing steps. TGA measurements of CNT@MS@IBAM-DOX were performed in the temperature range of 50-800°C and the result is presented in **Figure 4.C**. With CNT@MS@IBAM as the baseline, the amount of DOX loaded could be calculated; the TGA curve revealed a weight loss correlated to the DOX decomposition of ca. 56% of CNT@MS (see **Figure S3** for the TGA of DOX decomposition itself and **Table S1** for explanations about the calculations by TGA). This value is consistent with the DOX content calculated from UV/vis, considering that ca. loosely bound DOX was lost during washing steps. These DLC values are particularly high in the field of MS nanosystems as a usual range of 10-40% is reported, depending on the drug loading conditions [55–58]. We expect that in the case of IBAM grafts, a mechanism of drug-sponge effect similar to the one encountered with APTS in our previous work [42] may be the reason for such high drug loading.

Then, once the composite was suitably loaded with DOX, an HSA coating was directly added just after removing the impregnation supernatant. The adsorption of HSA in aqueous solution at a concentration of ca. 0.21 mg mL<sup>-1</sup> was performed on two CNT@MS@IBAM-DOX

nanocomposites with initial DOX loading measured at DLC = 18% and 34%. The quantification of the amount of HSA coated on the CNT@MS@IBAM-DOX composites was achieved and followed by spectrofluorimetry analysis of the supernatant. For that, HSA was labeled with the fluorophore FITC and a spectrofluorimetry calibration curve of HSA<sup>FITC</sup> (Exc/Em : 480/520 nm) in water measuring the fluorescence intensity emission at 520 nm at different HSA<sup>FITC</sup> concentrations was traced (**Figure S4**). Fluorescence spectra in **Figure 5.A** showed the complete disappearance in fluorescence at 520 nm of the supernatants after the HSA adsorption on both systems, which is compared to an HSA-FITC solution at 0.21 mg mL<sup>-1</sup>. This data showed that in the conditions of HSA adsorption, almost all the HSA brought in contact with the CNT@MS@IBAM-DOX composites was coated onto their surfaces, which was attributed to the non-covalent bonds between HSA and isobutyramide (IBAM) functional groups. This allowed us estimating that ca. 98 µg HSA was adsorbed per mg of CNT@MS composite. As observed above, some slight natural DOX leakage arose in both samples as DOX is highly soluble in water (cf slight signals at ca. 560 and 590 nm). After evaluation of the DOX amount loss by using the absorbance calibration curve, the final DLC of the drug tightly retained in the system after HSA coating and washing were found of 16 and 31% as compared to initial DOX loadings during DOX impregnation (DLC = 18% and 34%).

Regarding the surface charge, Zeta potential measurements as a function of the pH were performed on CNT@MS@IBAM@HSA and CNT@MS@IBAM-DOX@HSA systems (**Figure 5. B**) and very similar trends with and without DOX loading were found. The isoelectric point values for CNT@MS@IBAM@HSA and CNT@MS@IBAM-DOX@HSA (DLC = 56 %) composites were found at pH *ca.* 6 and 5, respectively. These data indicated that despite of the very high amount of DOX introduced, the surface charge is probably the same without and with DOX, which/and is mainly determined by the HSA coating. This confirms the good coverage of composites by HSA and its efficiency as gate-keeper.

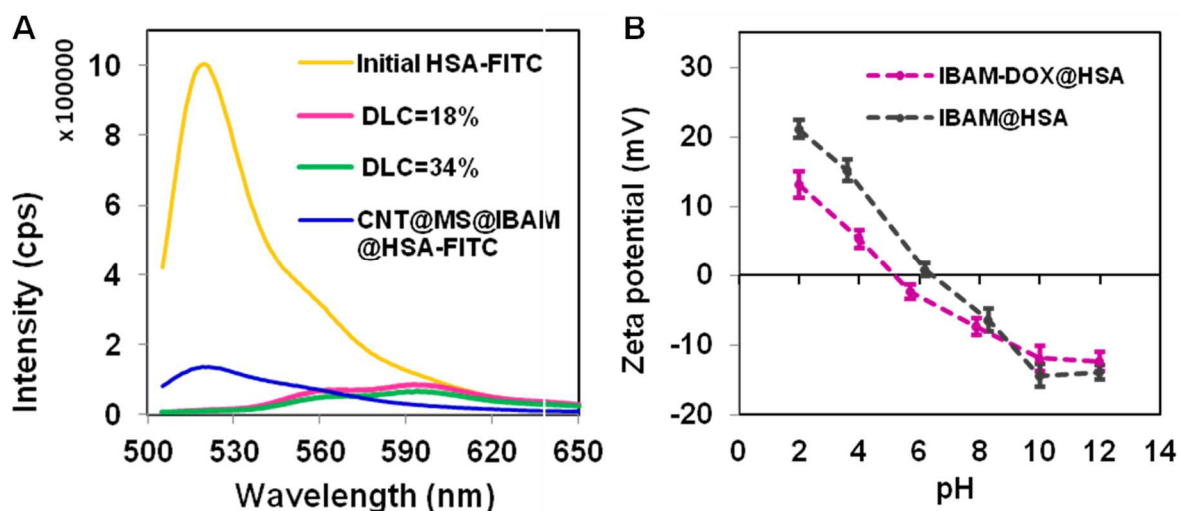


**Figure 5.** A) Fluorescence spectra of supernatant of CNT@MS@IBAM-DOX@HSA<sup>FITC</sup> (DLC = 18% and 34%), CTRL (CNT@MS@IBAM@HSA<sup>FITC</sup>) and HSA-FITC solution at 0.21 mg mL<sup>-1</sup>. B) Zeta potential curves as a function of pH for CNT@MS@IBAM-DOX@HSA and CNT@MS@IBAM@HSA.

#### 4. DOX Release

CNTs have strong absorbance in NIR region (in the range 750-1400 nm) and can convert the NIR light into local heat. By adding to their surface a thermally responsive coating, they become suitable photo-responsive nanostructures for the remote release of drugs. In this paragraph, we investigated the possibility to deliver DOX upon NIR photothermal effect. We assumed the generated heat would disturb intermolecular interactions between DOX and IBAM facilitating the DOX release.

To evaluate the photothermal properties, aqueous solutions (1 mL) of various concentrations of CNT@MS@IBAM-DOX@HSA (DLC ca. 58%) ranging from 0.32 to 2.5 mg mL<sup>-1</sup> (0.32; 0.63; 1.25 and 2.5 mg mL<sup>-1</sup>) were exposed to a 1064 nm NIR laser with power densities at 2.5 and 1 W cm<sup>-2</sup>. The temperature changes were then recorded as a function of time during the 15 min irradiation time of NIR light, as shown in **Figure 6.A** (2.5 W cm<sup>-2</sup>) and **6.B** (1 W cm<sup>-2</sup>). As expected, obvious photothermal heating of the suspensions were observed but with differences in terms of temperature profiles between the two powers used. At the highest NIR power density of 2.5 W cm<sup>-2</sup> (**Figure 6. A**), the temperature profiles of the suspensions were shown not to depend on the nanocomposite concentration and increased rapidly from ca. 31 to 68 °C at the early stage (over the first 5 minutes) and then remained substantially constant with extending exposure time. The effect of the NIR light in water (without CNTs composites) showed a slight increase of the T from 22 to 30 °C when exposure to the 2.5 W cm<sup>-2</sup> NIR laser, confirming a temperature effect of the composites. Oppositely, the temperature of the solution under 1 W cm<sup>-2</sup> NIR irradiation (**Figure 6. B**) increased slowly throughout the run and was found to be finely tunable with concentrations and irradiation times so that temperature could be raised in a



controlled manner from 28 to 41°C. The power effect is important when applied to cells to avoid their necrosis which is expected above 45 °C[59–61]. In contrast, by looking at the effect of the NIR light in the solution without composites, the temperature of pure water showed almost no changes under the same power condition. The excellent photothermal performances of CNTs whatever the power make them thusly an effective photothermal agent and we have now to demonstrate that it is efficient for drug delivery.

Then, the NIR-light controlled drug release properties of CNT@MS@IBAM-DOX@HSA were investigated by measuring the DOX amount released from the exposed suspensions (DLC = 58%) at various concentrations of (0.32 - 2.5 mg ml<sup>-1</sup>) under NIR laser for 15 min (followed by three days at rest at 4°C) at power densities of 1 and 2.5 W.cm<sup>-2</sup>. For each concentration, a control sample (CTRL) not exposed to NIR light at room temperature was also considered. The supernatants of the centrifuged suspensions after NIR treatment (and rest time) were monitored by UV/Vis absorption spectroscopy at 480 nm to determine the amount of DOX released during this period. As shown in **Figure 6.C**, the increased sample concentration resulted in an increased DOX release under NIR light stimulation at both power densities, 1 and 2.5 W cm<sup>-2</sup>, with very similar DOX release trends for both power densities. Hence after the first 15 min NIR irradiation trail, respectively ca. 21 and 22 µg of DOX were released at the concentration of 2.5 mg mL<sup>-1</sup> under NIR power densities of 2.5 and 1 W cm<sup>-2</sup>, respectively, which correspond to almost three times that of the control sample (natural leakage) of 8 µg. This natural release is attributed to a spontaneous desorption of DOX that occurs with time which remains however lower than that of the photo-induced one. A photograph of the supernatants (**Figure 6. D**) illustrated the differences in contrast of DOX between the samples submitted to NIR light and the control. Finally, regarding the results obtained in Figures 6.A and B for the T profiles and the results obtained in drug release in **Figures 6.C** and **D**, we can conclude that the NIR exposure at 1W.cm<sup>-2</sup> condition is optimal as it ensures a better T control and efficient drug release.

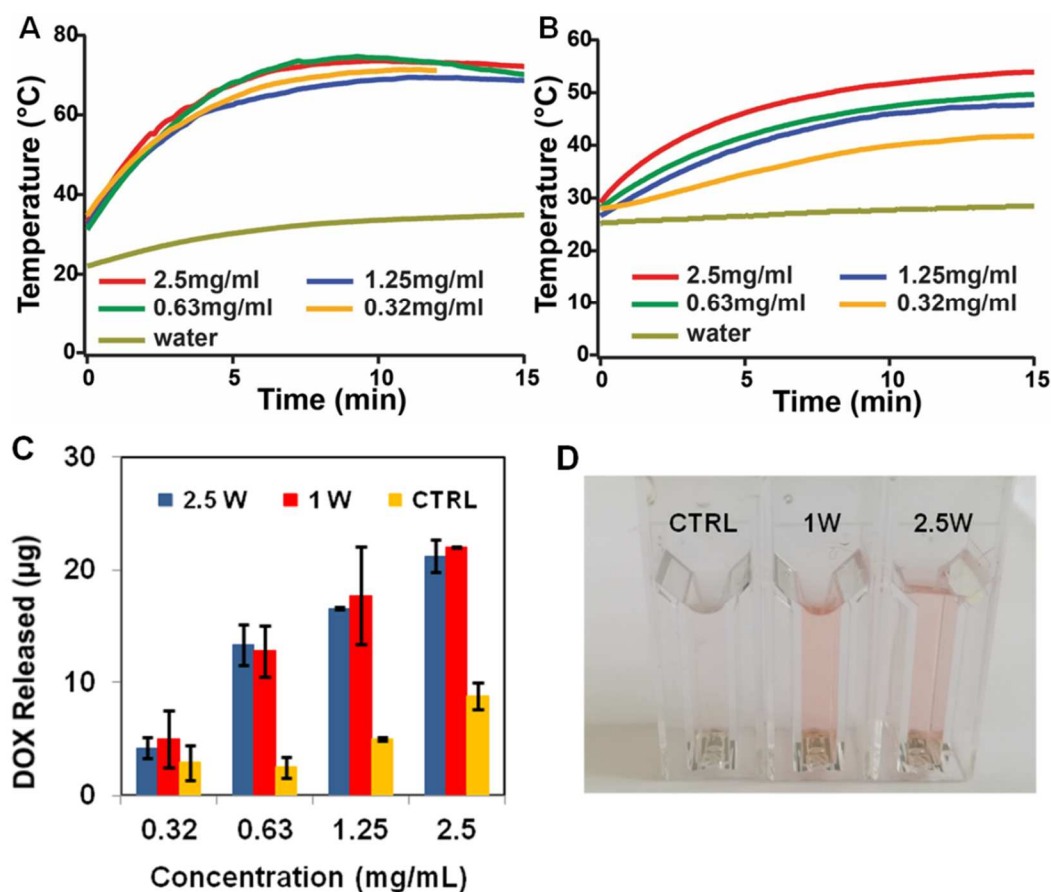


**Figure 6.** Changes in temperature of 1 mL of CNT@MS@IBAM-DOX@HSA (DLC = 58%) at various concentrations upon irradiation by the 1064 nm NIR laser at a power density of A) 2.5 W cm<sup>-2</sup> and B) 1 W cm<sup>-2</sup>. C) Mass of DOX released from various concentrations of CNT@MS@IBAM-DOX@HSA (DLC = 58%) upon NIR laser irradiation at power densities of 2.5 and 1 W cm<sup>-2</sup>, and ambient T (CTRL). D) Photograph of the DOX released from the composite concentration of 2.5 mg mL<sup>-1</sup> (DLC = 58%) after NIR exposure at the two power densities (1W and 2.5W) or when exposed to room T (CTRL)

We also investigated the effect of pulsatile release by performing four cycles of NIR laser irradiation to the four batches at various concentrations (0.32; 0.63; 1.25 and 2.5 mg ml<sup>-1</sup>). Pulsatile release is a very attractive approach because triggering the drug release in several pulses with chosen periods could be beneficial for a treatment needing dosing in several sequential steps of the drug administration.[62–65] As observed above, this system is supposed to have a continuous, rather slow release of DOX in the absence of NIR light, and the pulsatile release would ensure bursts of DOX released upon NIR irradiations. As shown in **Figure 7.A**, for nanocomposites at a concentration of 2.5 mg mL<sup>-1</sup> (DLC = 58%), along four consecutive NIR treatment cycles, the DOX release enhancement was found to be lower than for the first pulse reaching nevertheless a rate ca. 5 ug DOX/pulse. This can be explained by the observed

agglomeration of the CNT@MS@IBAM-DOX@HSA composite induced by NIR irradiation at the power density of  $2.5 \text{ W cm}^{-2}$ . Finally, the cumulative amount of DOX released was found to be of *ca.* 37 and  $34 \mu\text{g}$  upon NIR laser application at  $2.5$  and  $1 \text{ W cm}^{-2}$ , respectively. For  $1.25$ ,  $0.63$  and  $0.32 \text{ mg mL}^{-1}$  (**Figures 7.B-C-D**), the cumulative DOX release showed also a moderate though progressive increase after each cycle of NIR irradiation with the following slopes after the first pulse: *ca.* 4, 3, 2  $\mu\text{g DOX/NIR pulse}$ . Percentages of the cumulative release of DOX as compared to the initial loading of DOX in the CNT@MS@IBAM-DOX@HSA nanocomposites for all of these graphs are provided in **Figure S5**. Even if the DOX loading ( $58\%$  *i.e.*  $580 \mu\text{g.mg}^{-1}$  CNTS@MS) is very high as compared to the literature and the amount released in **Figure 7** are suitable for cancer cell toxicity, the % DOX amount released indicate that only less than 10% of the total DOX loaded amount is released. Nevertheless, this lets envisioning using these systems for long term and sustained pulsatile release. Altogether, these results showed that the amount of DOX released upon NIR is proportional to the composite concentration (at equal DLC). Moreover, since power of NIR had no substantial benefit on the amount of DOX that is released (see **Figure S5.A and B**), using low power (1W) allows to preserve a better temperature control below the inflammation/necrotic temperature of  $45^\circ\text{C}$  [59–61].

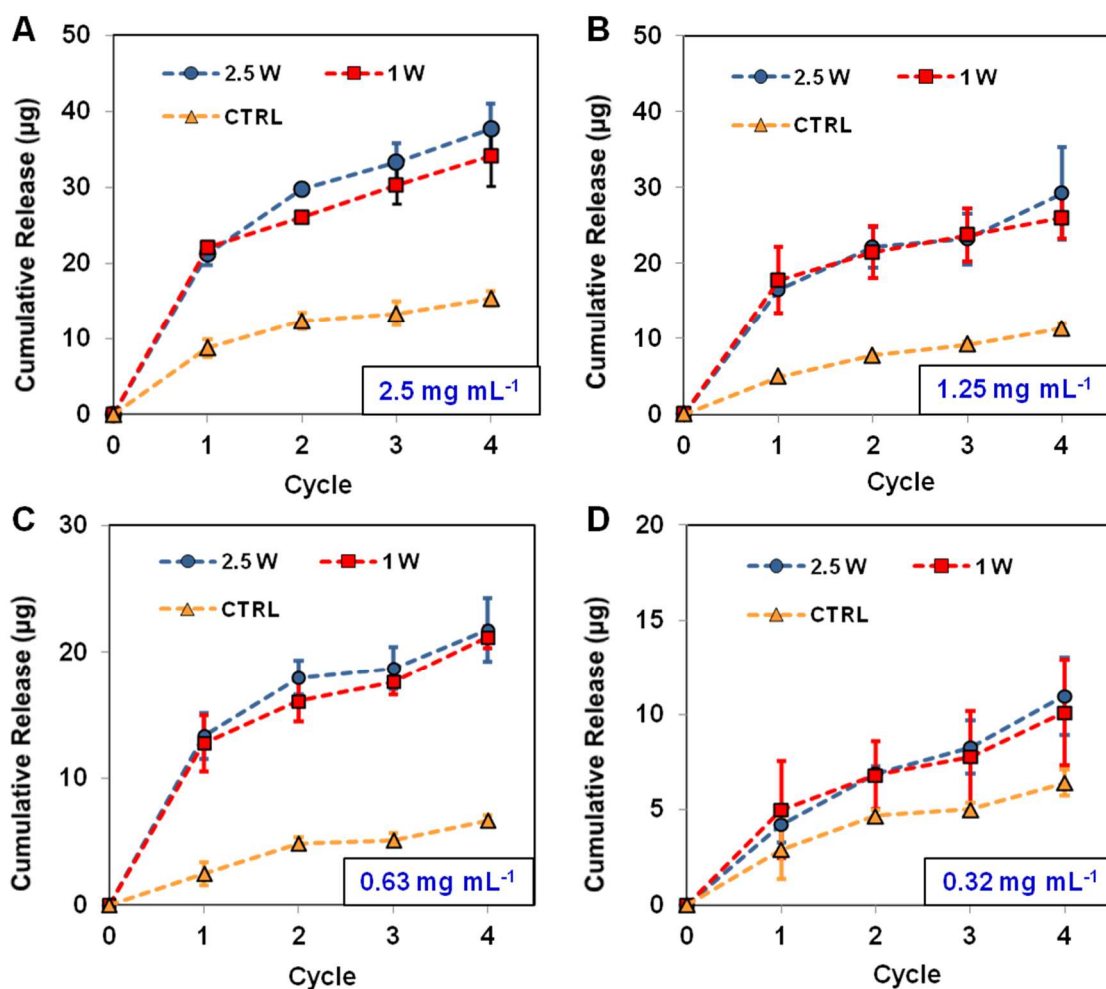


**Figure 7.** Cumulative DOX release from various concentrations of CNT@MS@IBAM-DOX@HSA: A) 2.5 mg mL<sup>-1</sup>, B) 1.25 mg mL<sup>-1</sup>, C) 0.63 mg mL<sup>-1</sup> and D) 0.32 mg mL<sup>-1</sup> (DLC = 58%) upon four consecutive NIR laser irradiation cycles at power densities of 2.5 and 1 W cm<sup>-2</sup> (15 min ON, 3 days OFF), and at ambient T (CTRL).

## 5. Uptake of DOX and cytotoxicity upon NIR excitation

Here, we aimed at testing the cytotoxic potential of our functionalized nanocomposites using a classical breast carcinoma tumor cell line. We tested its cytotoxic effect using either a (i) classical cell culture where CNTs are supplemented to the cell culture medium, or (ii) a hydrogel-composite formulation where the nanocomposites are dispersed in the hydrogel (Matrigel) on top of which cells are seeded.

Cytotoxicity of CNT@MS@IBAM@HSA (without DOX) and CNT@MS@IBAM-DOX@HSA-loaded cells without and with NIR irradiation was estimated at various concentrations (**Figure 8.A-C**). First, we observe a very little cytotoxicity of CNT@MS@IBAM@HSA on tumor cells when no NIR is applied (**Figure 8.A**, yellow curve), independently of the nanocomposite concentration. Indeed, without any irradiation, D2A1 cells treated with CNT@MS@IBAM@HSA are only poorly affected with an average viability that remains for the 4 concentration conditions over 90%. Interestingly, a dose-dependent cytotoxicity was observed when tumor cells were subjected to CNT@MS@IBAM-DOX@HSA (**Figure 8.A**, blue curve), that could arise from previously observed DOX leaking from the nanocomposites.

Upon NIR light, cytotoxicities of CNT@MS@IBAM@HSA and of CNT@MS@IBAMDOX@HSA were significantly increased suggesting that T increase is sufficient to promote a cytotoxic effect of the CNTs (**Figure 8.A** green and red curves). Indeed, if we compare nanocomposites loaded with DOX, CNT@MS@IBAM-DOX@HSA, under NIR irradiation with the one without DOX, the release of DOX appears to moderately enhance cellular death (DOX vs NO DOX under NIR light). However it can be observed that, we reached a very efficient cytotoxic effect when both NIR and CNT@MS@IBAMDOX@HSA are applied, demonstrating the synergistic effects of photothermia and DOX release. (**Figure 8.C**)

Noteworthy, as a control, we investigated also the NIR irradiation effect onto cells without the composites. NIR irradiation showed no significant cytotoxicity further indicating that the locally increase heat from the nanocomposites is required to induce subsequent cell death (**Figure S7.A**). In conclusion, cytotoxicity is predominantly mediated by CNTs-dependent local T° increase and it can be enhanced with DOX release.

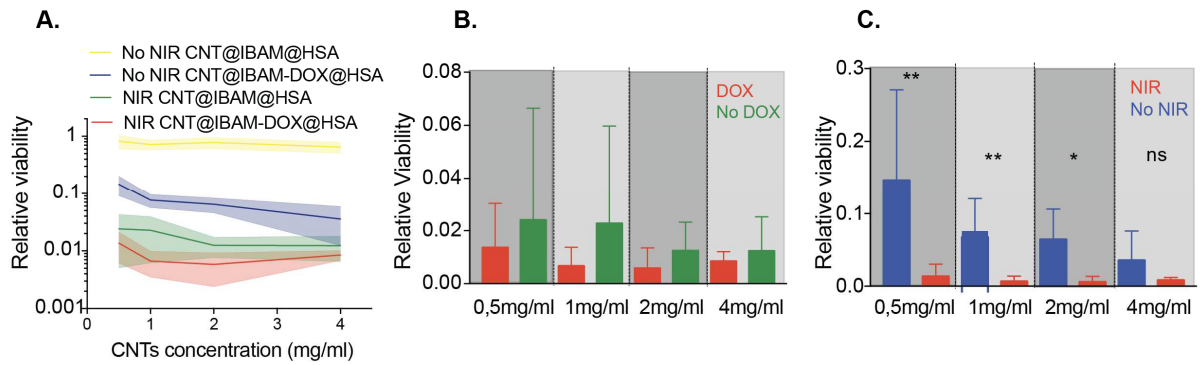


**Figure 8.** Viability assay results. A) The relative emission values in semi logarithmic scale as compared to the control (cells grown without nanocomposites) after 24 h of incubation with the nanocomposites followed by 15 min NIR irradiation. CNT@MS@IBAM@HSA (no DOX) and CNT@MS@IBAM-DOX@HSA (DOX) composites at concentrations 0.5, 1, 2, and 4 mg ml<sup>-1</sup> were considered. Represented on the graph are the average values and the SEM. B) Relative cellular viability extracted from graph A with and without DOX, upon 15 minutes of NIR exposure for CNT@MS@IBAM@HSA (no DOX) and CNT@MS@IBAM-DOX@HSA (DOX) at concentrations of 0.5, 1, 2, and 4 mg ml<sup>-1</sup>. C) Relative cellular viability with and without 15 minutes of NIR light exposure on CNT@MS@IBAM-DOX@HSA at the concentrations of 0.5, 1, 2 and 4mg ml<sup>-1</sup>,

With the aim to evidence that the DOX loaded in the CNT@MS@IBAM-DOX@HSA nanocomposites can be efficiently delivered to the cancer cells following NIR light application, thereby enhancing cytotoxic activity, we decided to incorporate the composites inside a 3D hydrogel scaffold. Additionally, this allows to shield cells from the unwanted non-specific adsorption of heat-inducing composite particles. Hence, the CNT@MS@IBAM-DOX@HSA nanocomposites were formulated within a commercially-available biocompatible protein-based hydrogel (Matrigel) that mimicks a biocompatible implantable scaffold. Indeed, the development of activable nanocomposite scaffolds has become an emerging field in nanomedicine and biomaterials which allows to solve issues associated with the use of injectable scaffolds (such as local injection, controlled release, limited loss of therapeutics). To build such nanocomposite scaffolds, CNT@MS@IBAM-DOX@HSA suspensions at 2 and 4 mg ml<sup>-1</sup> were mixed with Matrigel as substrates for the growth of the tumor cells and CNT@MS@IBAM@HSA were mixed to Matrigels to be used as controls. DOX release and uptake upon NIR was followed by confocal microscopy and the results showed significantly increased red fluorescence signals when cells were treated with CNT@MS@IBAM-DOX@HSA (**Figure 9.A, B and C**). The procedure allowing to visualize the cellular DOX uptake (red color) and the CNTs@MS@IBAM-DOX-HSA nanocomposites (white color) distribution is detailed in **Figure S8**. While absence of NIR led to backgrounds levels of DOX we observed a dose-dependent NIR-stimulated DOX release in tumor

cells (**Figure 9.A**). Overall, this confirms that DOX is released from the CNT@MS@IBAM-DOX@HSA nanocomposites upon NIR light application and that it contributes to synergistic effect of photothermia and DOX release observed in the 2C cell culture in the previous paragraph.

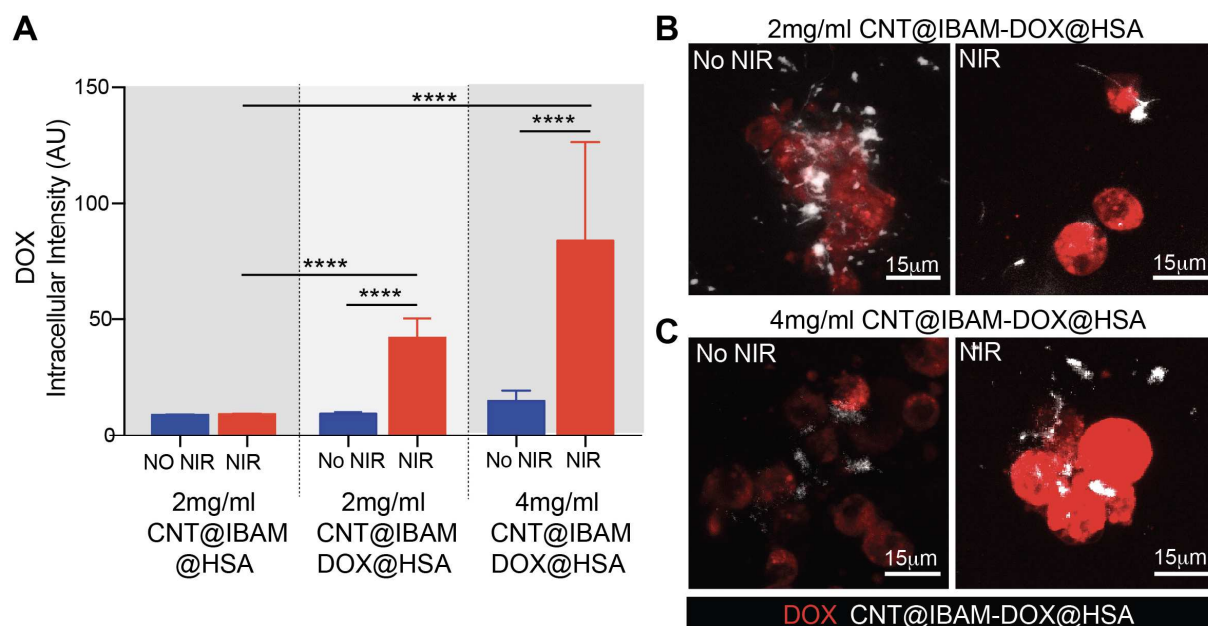


**Figure 9.** A) Intracellular DOX intensity. Average and standard deviation from the red DOX fluorescence signal in the different scaffold conditions. *P* values were calculated by the Mann Whitney test (\*\*\*\*  $p < 0.0001$ ). Z-projection of a fluorescent stack of images taken on D2A1 cells grown in CNT@IBAM-DOX@HSA composite at concentrations of B) 2 mg mL<sup>-1</sup> and C) 4 mg mL<sup>-1</sup> without and with NIR irradiation, respectively.

At last, to assess whether this hydrogel nanocomposite loaded with CNTs@MS@IBAM-DOX@HSA displays cytotoxicity towards murine breast cancer cells in 3D conditions, we assessed cellular growth in presence of different nanocomposites (**Figure 10**). The cells were grown over 5 days in either Matrigel (control without nanocomposites) or in a mixture of Matrigel added with the nanocomposites at 2.5 mg mL<sup>-1</sup>. While CNT@MS@IBAM@HSA had no effect on cellular growth as compared to the control without nanocomposites (**Fig.10A-B**), CNT@IBAM-DOX@HSA significantly lead to cell death in these conditions (**Fig.10C**). Thus, when incorporated into a matrix, CNTs@IBAM@HSA are not cytotoxic. When functionalized with DOX, its release would favor cytotoxicity (as expected upon NIR light). Such property could be beneficial for antitumor applications where drug release could be potentiated with an external stimulus such as NIR light.

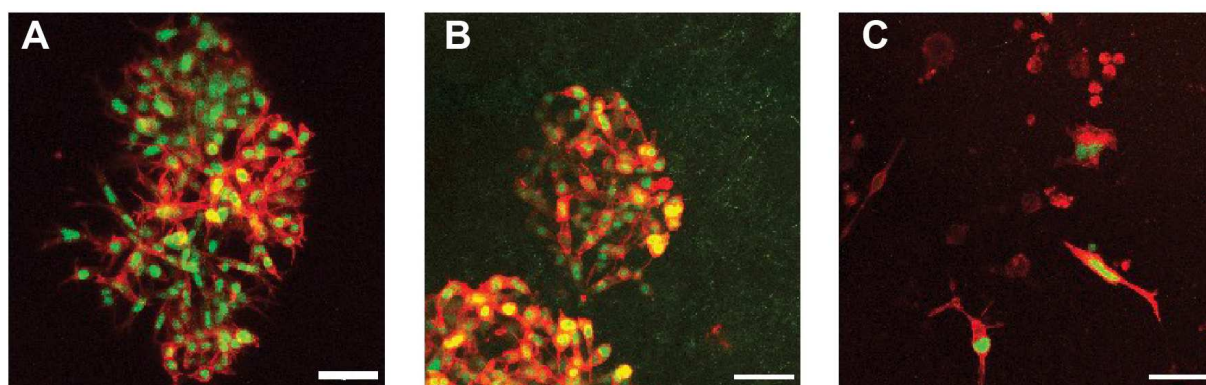


**Figure 10.** Confocal microscopy imaging of 3D tumoral D2A1 cancer cell growth in Matrigel over 5 days in the absence or in the presence of the nanocomposites. D2A1 grown) in Matrigel (A) in the absence of nanocomposites (B) treated with  $2.5 \text{ mg mL}^{-1}$  CNT@MS@IBAM@HSA and (C) treated with  $2.5 \text{ mg mL}^{-1}$  CNT@MS@IBAM-DOX@HSA. (scale bars  $50 \mu\text{m}$ ). (C) In green : the nuclear localization signal and in red : the actin filaments.

## Conclusion

In this work, we have designed new NIR light-responsive nanocomposites made of MS shell coated CNTs, loaded with the antitumor drug doxorubicin (DOX), and capped with plasma protein human serum albumin (HSA) as a biocompatible interface and gate keeper. We have developed here a novel way to immobilize DOX with a DLC up to 80%, (a very high amount as compared to the literature), via the powerful strategy based on IBAM versatile non-covalent binders grafted on CNT@MS shells which additionally allow the tight anchoring of HSA .

The photothermal properties of these composites were investigated as a function of their concentration and of the laser power. We found that adjusting the power at  $1 \text{ W.cm}^2$  is well suited to control the temperature under the necrosis temperature ( $45^\circ\text{C}$ ). These drug loaded CNTs@MS@IBAM-DOX-HSA nanocomposites were shown to release DOX in response to NIR light applied. We demonstrated that this release occurs first by a burst that depends on the concentration of the composites but can also be controlled on a pulsatile fashion as a regular increase of DOX occurs after each NIR light application. We demonstrated that a NIR power of  $1 \text{ W.cm}^{-2}$  is efficient to control the release of DOX dose on time.

We further demonstrated the cytotoxic potential of DOX-loaded nanocomposites and highlighted a potentially interesting feature of our nanocomposites: even if photothermic effect from the CNTs composites allows an important cancer cell cytotoxicity, the DOX -mediated release ensure an additional cytotoxicity allowing synergy of both effect to kill cancer cells. Finally, another originality of this work is the integration of such nanocomposites into a hydrogel mimicking the extracellular matrix which can have potential applications in the field of antitumoral scaffolds or polymer matrices for tissue engineering (if DOX is replaced by another

molecule). We showed here that the application of NIR light on such nanocomposite hydrogel scaffold covered with D2A1 murine breast cancer cells allows triggering the release of DOX to the cellular media, which results in cell toxicity over time.

Hence, such nanosystems may be of huge interest as components of implantable scaffolds for antitumor or tissue engineering applications. This approach would make it possible the development of new (nano) medical devices for the medicine of tomorrow.

### **Data availability.**

The raw/processed data required to produce these findings can be shared on demand.

### **Author contributions.**

The manuscript was written with contributions of all authors. All authors have given approval to the final version of the manuscript.

### **Acknowledgements**

D.M. acknowledges the Materials Institute Carnot Alsace (project ProtRemote) and the Canceropôle Est (project VIVIRMAG) for the financial supports. Bing LI would like to thank the Chinese Scholarship Council (CSC) for the grant during her PhD at the University of Strasbourg. M.T. acknowledges CONICET for funding and support for researchers' exchange, as well as the EU project Hygraphen for researchers' mobility allowances. Work in the Goetz lab (VG, SH, JGG) is supported by institutional funds from INSERM and University of Strasbourg as well as by Canceropôle Est (project VIVIRMAG). V.G. funded by an INSERM/RegionEst *Ph.D.* fellowship.

### **Bibliography**

- [1] S. Augustine, J. Singh, M. Srivastava, M. Sharma, A. Das, B.D. Malhotra, Recent advances in carbon based nanosystems for cancer theranostics, *Biomater. Sci.* 5 (2017) 901–952. <https://doi.org/10.1039/C7BM00008A>.
- [2] E. Cazares-Cortes, S. Cabana-Montenegro, C. Boitard, E. Nehling, N. Griffete, J. Fresnais, C. Wilhelm, A. Abou-Hassan, C. Ménager, Recent insights in magnetic hyperthermia: From the “hot-spot” effect for local delivery to combined magneto-photo-thermia using magneto-plasmonic hybrids, *Adv. Drug Deliv. Rev.* (2018).
- [3] S. Kralj, T. Potrc, P. Kocbek, S. Marchesan, D. Makovec, Design and fabrication of magnetically responsive nanocarriers for drug delivery, *Curr. Med. Chem.* 24 (2017) 454–469.
- [4] D. Mertz, O. Sandre, S. Bégin-Colin, Drug releasing nanoplatforms activated by alternating magnetic fields, *Biochim. Biophys. Acta BBA - Gen. Subj.* 1861 (2017) 1617–1641. <https://doi.org/10.1016/j.bbagen.2017.02.025>.
- [5] S. Mura, J. Nicolas, P. Couvreur, Stimuli-responsive nanocarriers for drug delivery, *Nat. Mater.* 12 (2013) 991–1003. <https://doi.org/10.1038/nmat3776>.
- [6] M.A.C. Stuart, W.T.S. Huck, J. Genzer, M. Müller, C. Ober, M. Stamm, G.B. Sukhorukov, I. Szleifer, V.V. Tsukruk, M. Urban, F. Winnik, S. Zauscher, I. Luzinov, S. Minko, *Emerging*



- applications of stimuli-responsive polymer materials, *Nat. Mater.* 9 (2010) 101–113. <https://doi.org/10.1038/nmat2614>.
- [7] A.K. Gaharwar, N.A. Peppas, A. Khademhosseini, Nanocomposite hydrogels for biomedical applications, *Biotechnol. Bioeng.* 111 (2014) 441–453. <https://doi.org/10.1002/bit.25160>.
- [8] L. Gao, L. Xia, R. Zhang, D. Duan, X. Liu, J. Xu, L. Luo, Enhanced antitumor efficacy of poly (D, L-lactide-co-glycolide)-based methotrexate-loaded implants on sarcoma 180 tumor-bearing mice, *Drug Des. Devel. Ther.* 11 (2017) 3065.
- [9] N.S. Satarkar, D. Biswal, J.Z. Hilt, Hydrogel nanocomposites: a review of applications as remote controlled biomaterials, *Soft Matter*. 6 (2010) 2364–2371.
- [10] S. Talebian, J. Foroughi, S.J. Wade, K.L. Vine, A. Dolatshahi-Pirouz, M. Mehrali, J. Conde, G.G. Wallace, Biopolymers for Antitumor Implantable Drug Delivery Systems: Recent Advances and Future Outlook, *Adv. Mater.* 30 (2018) 1706665. <https://doi.org/10.1002/adma.201706665>.
- [11] B.D. Weinberg, E. Blanco, J. Gao, Polymer implants for intratumoral drug delivery and cancer therapy, *J. Pharm. Sci.* 97 (2008) 1681–1702.
- [12] Y. Zhang, J. Yu, H.N. Bomba, Y. Zhu, Z. Gu, Mechanical Force-Triggered Drug Delivery, *Chem. Rev.* 116 (2016) 12536–12563. <https://doi.org/10.1021/acs.chemrev.6b00369>.
- [13] D. Mertz, S. Harlepp, J. Goetz, D. Bégin, G. Schlatter, S. Bégin-Colin, A. Hébraud, Nanocomposite Polymer Scaffolds Responding under External Stimuli for Drug Delivery and Tissue Engineering Applications, *Adv. Ther.* n/a (n.d.) 1900143. <https://doi.org/10.1002/adtp.201900143>.
- [14] S. Merino, C. Martín, K. Kostarelos, M. Prato, E. Vázquez, Nanocomposite Hydrogels: 3D Polymer–Nanoparticle Synergies for On-Demand Drug Delivery, *ACS Nano*. 9 (2015) 4686–4697. <https://doi.org/10.1021/acsnano.5b01433>.
- [15] A.A. Adedoyin, A.K. Ekenseair, Biomedical applications of magneto-responsive scaffolds, *Nano Res.* 11 (2018) 5049–5064. <https://doi.org/10.1007/s12274-018-2198-2>.
- [16] A. Battigelli, C. Ménard-Moyon, T. Da Ros, M. Prato, A. Bianco, Endowing carbon nanotubes with biological and biomedical properties by chemical modifications, *Adv. Drug Deliv. Rev.* 65 (2013) 1899–1920.
- [17] H. Gong, R. Peng, Z. Liu, Carbon nanotubes for biomedical imaging: the recent advances, *Adv. Drug Deliv. Rev.* 65 (2013) 1951–1963.
- [18] H. Dai, Carbon nanotubes: synthesis, integration, and properties, *Acc. Chem. Res.* 35 (2002) 1035–1044.
- [19] A. Bianco, K. Kostarelos, C.D. Partidos, M. Prato, Biomedical applications of functionalised carbon nanotubes, *Chem. Commun.* (2005) 571–577.
- [20] K. Kostarelos, A. Bianco, M. Prato, Promises, facts and challenges for carbon nanotubes in imaging and therapeutics, *Nat. Nanotechnol.* 4 (2009) 627–633.
- [21] Z. Liu, J.T. Robinson, S.M. Tabakman, K. Yang, H. Dai, Carbon materials for drug delivery & cancer therapy, *Mater. Today*. 14 (2011) 316–323.
- [22] R. Singh, S.V. Torti, Carbon nanotubes in hyperthermia therapy, *Adv. Drug Deliv. Rev.* 65 (2013) 2045–2060.
- [23] B.S. Wong, S.L. Yoong, A. Jagusiak, T. Panczyk, H.K. Ho, W.H. Ang, G. Pastorin, Carbon nanotubes for delivery of small molecule drugs, *Adv. Drug Deliv. Rev.* 65 (2013) 1964–2015.
- [24] C. Ge, J. Du, L. Zhao, L. Wang, Y. Liu, D. Li, Y. Yang, R. Zhou, Y. Zhao, Z. Chai, Binding of blood proteins to carbon nanotubes reduces cytotoxicity, *Proc. Natl. Acad. Sci.* 108 (2011) 16968–16973.
- [25] B. Koh, W. Cheng, Mechanisms of Carbon Nanotube Aggregation and the Reversion of Carbon Nanotube Aggregates in Aqueous Medium, *Langmuir*. 30 (2014) 10899–10909. <https://doi.org/10.1021/la5014279>.
- [26] X. Wang, T. Xia, S.A. Ntim, Z. Ji, S. George, H. Meng, H. Zhang, V. Castranova, S. Mitra, A.E. Nel, Quantitative Techniques for Assessing and Controlling the Dispersion and Biological Effects of Multiwalled Carbon Nanotubes in Mammalian Tissue Culture Cells, *ACS Nano*. 4 (2010) 7241–7252. <https://doi.org/10.1021/nn102112b>.

- [27] H.B. Chew, M.-W. Moon, K.R. Lee, K.-S. Kim, Compressive dynamic scission of carbon nanotubes under sonication: fracture by atomic ejection, in: Proc. R. Soc. Lond. Math. Phys. Eng. Sci., The Royal Society, 2011: pp. 1270–1289.
- [28] J. Liu, A.G. Rinzler, H. Dai, J.H. Hafner, R.K. Bradley, P.J. Boul, A. Lu, T. Iverson, K. Shelimov, C.B. Huffman, Fullerene pipes, *Science*. 280 (1998) 1253–1256.
- [29] X. Liu, R.H. Hurt, A.B. Kane, Biodurability of single-walled carbon nanotubes depends on surface functionalization, *Carbon*. 48 (2010) 1961–1969. <https://doi.org/10.1016/j.carbon.2010.02.002>.
- [30] Z. Liu, X. Sun, N. Nakayama-Ratchford, H. Dai, Supramolecular chemistry on water-soluble carbon nanotubes for drug loading and delivery, *ACS Nano*. 1 (2007) 50–56.
- [31] Z. Liu, K. Chen, C. Davis, S. Sherlock, Q. Cao, X. Chen, H. Dai, Drug delivery with carbon nanotubes for in vivo cancer treatment, *Cancer Res*. 68 (2008) 6652–6660.
- [32] Z. Liu, A.C. Fan, K. Rakhra, S. Sherlock, A. Goodwin, X. Chen, Q. Yang, D.W. Felsner, H. Dai, Supramolecular stacking of doxorubicin on carbon nanotubes for in vivo cancer therapy, *Angew. Chem. Int. Ed*. 48 (2009) 7668–7672.
- [33] M. Zheng, A. Jagota, E.D. Semke, B.A. Diner, R.S. Mclean, S.R. Lustig, R.E. Richardson, N.G. Tassi, DNA-assisted dispersion and separation of carbon nanotubes, *Nat. Mater*. 2 (2003) 338–342. <https://doi.org/10.1038/nmat877>.
- [34] M. Zhang, X. Zhang, X. He, L. Chen, Y. Zhang, A facile method to coat mesoporous silica layer on carbon nanotubes by anionic surfactant, *Mater. Lett*. 64 (2010) 1383–1386.
- [35] K. Ding, B. Hu, Y. Xie, G. An, R. Tao, H. Zhang, Z. Liu, A simple route to coat mesoporous SiO<sub>2</sub> layer on carbon nanotubes, *J. Mater. Chem*. 19 (2009) 3725–3731.
- [36] S.-W. Bian, Z. Ma, L.-S. Zhang, F. Niu, W.-G. Song, Silica nanotubes with mesoporous walls and various internal morphologies using hard/soft dual templates, *Chem. Commun.* (2009) 1261–1263.
- [37] P. Yang, S. Gai, J. Lin, Functionalized mesoporous silica materials for controlled drug delivery, *Chem. Soc. Rev*. 41 (2012) 3679–3698.
- [38] M. Ménard, F. Meyer, K. Parkhomenko, C. Leuvrey, G. Francius, S. Bégin-Colin, D. Mertz, Mesoporous silica templated-albumin nanoparticles with high doxorubicin payload for drug delivery assessed with a 3-D tumor cell model, *Biochim. Biophys. Acta BBA - Gen. Subj*. 1863 (2019) 332–341. <https://doi.org/10.1016/j.bbagen.2018.10.020>.
- [39] F. Perton, S. Harlepp, G. Follain, K. Parkhomenko, J.G. Goetz, S. Bégin-Colin, D. Mertz, Wrapped stellate silica nanocomposites as biocompatible luminescent nanoplatforms assessed in vivo, *J. Colloid Interface Sci*. 542 (2019) 469–482. <https://doi.org/10.1016/j.jcis.2019.01.098>.
- [40] M. Ménard, F. Meyer, C. Affolter-Zbaraszczuk, M. Rabineau, A. Adam, P.D. Ramirez, S. Bégin-Colin, D. Mertz, Design of hybrid protein-coated magnetic core-mesoporous silica shell nanocomposites for MRI and drug release assessed in a 3D tumor cell model, *Nanotechnology*. 30 (2019) 174001. <https://doi.org/10.1088/1361-6528/aafe1c>.
- [41] V. Fiegel, S. Harlepp, S. Bégin-Colin, D. Bégin, D. Mertz, Design of Protein-Coated Carbon Nanotubes Loaded with Hydrophobic Drugs through Sacrificial Templating of Mesoporous Silica Shells, *Chem. – Eur. J*. 24 (2018) 4662–4670. <https://doi.org/10.1002/chem.201705845>.
- [42] C. Wells, O. Vollin-Bringel, V. Fiegel, S. Harlepp, B.V. der Schueren, S. Bégin-Colin, D. Bégin, D. Mertz, Engineering of Mesoporous Silica Coated Carbon-Based Materials Optimized for an Ultrahigh Doxorubicin Payload and a Drug Release Activated by pH, T, and NIR-light, *Adv. Funct. Mater*. 28 (2018) 1706996. <https://doi.org/10.1002/adfm.201706996>.
- [43] F. Perton, M. Tasso, G.A. Muñoz Medina, M. Ménard, C. Blanco-Andujar, E. Portiansky, M.B.F. van Raap, D. Bégin, F. Meyer, S. Bégin-Colin, D. Mertz, Fluorescent and magnetic stellate mesoporous silica for bimodal imaging and magnetic hyperthermia, *Appl. Mater. Today*. 16 (2019) 301–314. <https://doi.org/10.1016/j.apmt.2019.06.006>.
- [44] D. Mertz, P. Tan, Y. Wang, T.K. Goh, A. Blencowe, F. Caruso, Bromoisobutyramide as an Intermolecular Surface Binder for the Preparation of Free-standing Biopolymer Assemblies, *Adv. Mater*. 23 (2011) 5668–5673. <https://doi.org/10.1002/adma.201102890>.

- [45] D. Mertz, J. Cui, Y. Yan, G. Devlin, C. Chaubaroux, A. Dochter, R. Alles, P. Lavalle, J.C. Voegel, A. Blencowe, Protein capsules assembled via isobutyramide grafts: sequential growth, biofunctionalization, and cellular uptake, *ACS Nano*. 6 (2012) 7584–7594.
- [46] D. Mertz, H. Wu, J.S. Wong, J. Cui, P. Tan, R. Alles, F. Caruso, Ultrathin, bioresponsive and drug-functionalized protein capsules, *J. Mater. Chem.* 22 (2012) 21434–21442.
- [47] S.H. Lü, Q. Lin, Y.N. Liu, Q. Gao, T. Hao, Y. Wang, J. Zhou, H. Wang, Z. Du, J. Wu, C.Y. Wang, Self-assembly of renal cells into engineered renal tissues in collagen/Matrigel scaffold in vitro, *J. Tissue Eng. Regen. Med.* 6 (2012) 786–792. <https://doi.org/10.1002/term.484>.
- [48] Y. Kimura, M. Ozeki, T. Inamoto, Y. Tabata, Time Course of de Novo Adipogenesis in Matrigel by Gelatin Microspheres Incorporating Basic Fibroblast Growth Factor, *Tissue Eng.* 8 (2002) 603–613. <https://doi.org/10.1089/107632702760240526>.
- [49] M.W. Laschke, M. Rücker, G. Jensen, C. Carvalho, R. Mülhaupt, N.-C. Gellrich, M.D. Menger, Incorporation of growth factor containing Matrigel promotes vascularization of porous PLGA scaffolds, *J. Biomed. Mater. Res. A*. 85A (2008) 397–407. <https://doi.org/10.1002/jbm.a.31503>.
- [50] G. Follain, N. Osmani, A.S. Azevedo, G. Allio, L. Mercier, M.A. Karreman, G. Solecki, M.J. Garcia León, O. Lefebvre, N. Fekonja, C. Hille, V. Chabannes, G. Dollé, T. Metivet, F.D. Hovsepian, C. Prudhomme, A. Pichot, N. Paul, R. Carapito, S. Bahram, B. Ruthensteiner, A. Kemmling, S. Siemonsen, T. Schneider, J. Fiehler, M. Glatzel, F. Winkler, Y. Schwab, K. Pantel, S. Harlepp, J.G. Goetz, Hemodynamic Forces Tune the Arrest, Adhesion, and Extravasation of Circulating Tumor Cells, *Dev. Cell*. 45 (2018) 33-52.e12. <https://doi.org/10.1016/j.devcel.2018.02.015>.
- [51] N. Osmani, G. Follain, M.J. García León, O. Lefebvre, I. Busnelli, A. Larnicol, S. Harlepp, J.G. Goetz, Metastatic Tumor Cells Exploit Their Adhesion Repertoire to Counteract Shear Forces during Intravascular Arrest, *Cell Rep.* 28 (2019) 2491-2500.e5. <https://doi.org/10.1016/j.celrep.2019.07.102>.
- [52] M. Vinci, S. Gowan, F. Boxall, L. Patterson, M. Zimmermann, W. Court, C. Lomas, M. Mendiola, D. Hardisson, S.A. Eccles, Advances in establishment and analysis of three-dimensional tumor spheroid-based functional assays for target validation and drug evaluation, *BMC Biol.* 10 (2012) 29. <https://doi.org/10.1186/1741-7007-10-29>.
- [53] X.-Y. Wang, D. Mertz, C. Blanco-Andujar, A. Bora, M. Ménard, F. Meyer, C. Giraudeau, S. Bégin-Colin, Optimizing the silanization of thermally-decomposed iron oxide nanoparticles for efficient aqueous phase transfer and MRI applications, *RSC Adv.* 6 (2016) 93784–93793.
- [54] D. Mertz, C. Affolter-Zbaraszcuk, J. Barthès, J. Cui, F. Caruso, T.F. Baumert, J.-C. Voegel, J. Ogier, F. Meyer, Templated assembly of albumin-based nanoparticles for simultaneous gene silencing and magnetic resonance imaging, *Nanoscale*. 6 (2014) 11676–11680.
- [55] N.Ž. Knežević, I.I. Slowing, V.S.-Y. Lin, Tuning the release of anticancer drugs from magnetic iron oxide/mesoporous silica core/shell nanoparticles, *ChemPlusChem*. 77 (2012) 48–55.
- [56] L. Yuan, Q. Tang, D. Yang, J.Z. Zhang, F. Zhang, J. Hu, Preparation of pH-responsive mesoporous silica nanoparticles and their application in controlled drug delivery, *J. Phys. Chem. C*. 115 (2011) 9926–9932.
- [57] J. Shen, Q. He, Y. Gao, J. Shi, Y. Li, Mesoporous silica nanoparticles loading doxorubicin reverse multidrug resistance: performance and mechanism, *Nanoscale*. 3 (2011) 4314–4322.
- [58] J. Liu, C. Detrembleur, M.-C. De Pauw-Gillet, S. Mornet, L. Vander Elst, S. Laurent, C. Jérôme, E. Duguet, Heat-triggered drug release systems based on mesoporous silica nanoparticles filled with a maghemite core and phase-change molecules as gatekeepers, *J. Mater. Chem. B*. 2 (2014) 59–70.
- [59] B.V. Harmon, A.M. Corder, R.J. Collins, G.C. Gobé, J. Allen, D.J. Allan, J.F.R. Kerr, Cell Death Induced in a Murine Mastocytoma by 42–47°C Heating in Vitro: Evidence that the Form of Death Changes from Apoptosis to Necrosis Above a Critical Heat Load, *Int. J. Radiat. Biol.* 58 (1990) 845–858. <https://doi.org/10.1080/09553009014552221>.
- [60] S. Li, S. Chien, P.-I. Brånemark, Heat shock-induced necrosis and apoptosis in osteoblasts, *J. Orthop. Res.* 17 (1999) 891–899. <https://doi.org/10.1002/jor.1100170614>.

- [61] S.S. Mambula, D. >Stuart K. Calderwood, Heat induced release of Hsp70 from prostate carcinoma cells involves both active secretion and passive release from necrotic cells, *Int. J. Hyperthermia*. 22 (2006) 575–585. <https://doi.org/10.1080/02656730600976042>.
- [62] J. Wu, A. Chen, M. Qin, R. Huang, G. Zhang, B. Xue, J. Wei, Y. Li, Y. Cao, W. Wang, Hierarchical construction of a mechanically stable peptide–graphene oxide hybrid hydrogel for drug delivery and pulsatile triggered release in vivo, *Nanoscale*. 7 (2015) 1655–1660. <https://doi.org/10.1039/C4NR05798H>.
- [63] J. Liu, C. Wang, X. Wang, X. Wang, L. Cheng, Y. Li, Z. Liu, Mesoporous Silica Coated Single-Walled Carbon Nanotubes as a Multifunctional Light-Responsive Platform for Cancer Combination Therapy, *Adv. Funct. Mater.* 25 (2015) 384–392.
- [64] W.-L. Chiang, C.-J. Ke, Z.-X. Liao, S.-Y. Chen, F.-R. Chen, C.-Y. Tsai, Y. Xia, H.-W. Sung, Pulsatile drug release from PLGA hollow microspheres by controlling the permeability of their walls with a magnetic field, *Small*. 8 (2012) 3584–3588.
- [65] Magneto-responsive Smart Capsules Formed with Polyelectrolytes, Lipid Bilayers and Magnetic Nanoparticles | *ACS Applied Materials & Interfaces*, (n.d.). <https://pubs.acs.org/doi/abs/10.1021/am900784a> (accessed January 29, 2020).

